Materials Science in Semiconductor Processing 174 (2024) 108227

Contents lists available at ScienceDirect

Materials Science in Semiconductor Processing

journal homepage: www.elsevier.com/locate/mssp

Electron emission from alignment-controlled multiple stacks of SiGe nanodots embedded in Si structures

Katsunori Makihara [a,*], Yuji Yamamoto [b], Hiroya Yagi [a], Lingrui Li [a], Noriyuki Taoka [c], Bernd Tillack [b,d], Seiichi Miyazaki [a]

[a] Graduate School of Engineering, Nagoya University, Furo–cho, Chikusa–ku, Nagoya, 464–8603, Japan
[b] IHP – Leibniz–Institut für Innovative Mikroelektronik, Im Technologiepark 25, Frankfurt, (Oder), 15236, Germany
[c] Aichi Institute of Technology, 1247 Yachigusa, Yakusa–cho, Toyota, 470–0356, Japan
[d] Technische Universität Berlin, HFT4, Einsteinufer 25, Berlin, 10587, Germany

ARTICLE INFO

Keywords:
SiGe Nanodots
Electron Emission

ABSTRACT

We fabricated a vertically aligned and staggered structure comprising 20–stacking layers of SiGe–nanodots (NDs) embedded in Si via reduced–pressure chemical vapor deposition and investigated their electron emission properties. The SiGe–NDs with a 35% Ge content were deposited using SiH_4–GeH_4, while Si spacers were deposited using SiH_4 or SiH_2Cl_2 to control a 3D–alignment of staggered or dot–on–dot structure, respectively. Top Au electrodes with 5–nm–thick SiO_2 and bottom Al contact were fabricated for electron emission measurements. After applying a bias of −3.8 V to the bottom Al–electrode with respect to the grounded top Au–electrode, electron emission was observed from the staggered SiGe–ND stack, which was slightly lower than that of the vertically–aligned NDs. In addition, we also observed a reduction in sample current with the formation of the staggered SiGe–ND stack. These results indicate that aligning SiGe–NDs in a staggered configuration suppresses leakage current and improves electron emission efficiency.

1. Introduction

The fabrication of SiGe– and Ge–nanodots (NDs) and their stack structures embedded in Si via controlling self–assembly in the early stages of heteroepitaxial growth on crystalline Si (c–Si) has attracted considerable attention because of their importance in practical applications, such as light–emitting diodes, mid–infrared photodetectors, and functional nanodevices with quantum transport [1–20]. Especially, electron field emission from Si–NDs has been intensively studied because its unique electron emission properties are expected to be suitable for electron microscope, electron lithography and field emission display [21–26]. In addition, the liquid–phase depositions of Si and Ge films have been successfully demonstrated by using a hot electron emitter based on the Si–NDs [27–29]. However, achieving precise control of NDs in three dimensions is critical to enabling smooth carrier transport. Therefore, the process development for heteroepitaxial growth of SiGe– and Ge–NDs on Si (001) is widely investigated using chemical vapor deposition (CVD) [30–33]. Previous studies have successfully demonstrated three–dimensional (3D) alignment control of SiGe–NDs. Using Si_2H_6 as a precursor for Si–spacer deposition, SiGe–NDs were formed directly above the embedded SiGe–NDs nearest to the Si surface (dot–on–dot), resulting in vertically aligned SiGe–NDs [34]. When SiH_4 was used for Si–spacer deposition, SiGe–NDs were formed on the Si surface with a checkerboard pattern [35,36]. By repeating the sequence of ND formation and Si–spacer deposition, SiGe–NDs were aligned at staggered positions. Nanobeam diffraction analysis revealed that the driving force behind this alignment is likely the local tensile strain formed at the Si surface above the embedded SiGe–ND. In this study, we fabricated vertically aligned and staggered structures comprising 20–stacked SiGe–NDs embedded in Si using a reduced–pressure (RP) CVD and characterized their electron emission properties.

2. Sample preparation

Self–ordered 3D SiGe–NDs embedded in Si structures were fabricated using RP–CVD. Herein, an n–type Si(100) wafer with a phosphorus concentration of $\sim 5 \times 10^{15}$ cm^{-3} was used. After conventional

* Corresponding author.
E-mail address: makihara@nuee.nagoya-u.ac.jp (K. Makihara).

https://doi.org/10.1016/j.mssp.2024.108227
Received 12 December 2023; Received in revised form 24 January 2024; Accepted 7 February 2024
Available online 22 February 2024

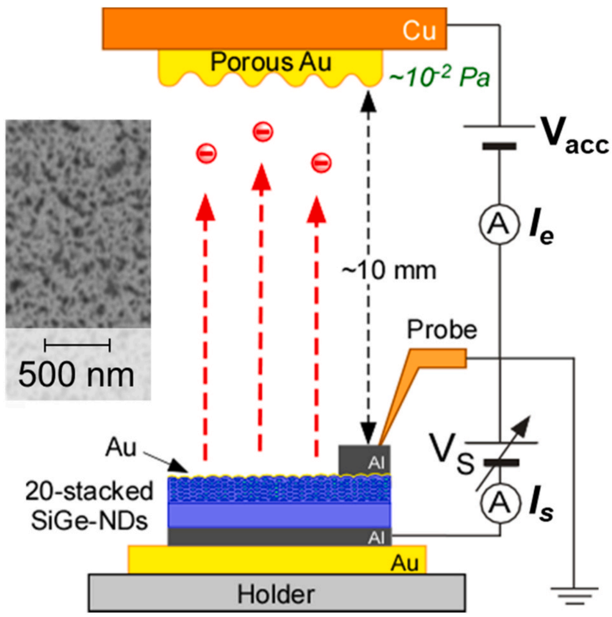

Fig. 1. Schematic view of measurement setup, and device structure. A SEM image of porous gold film is also shown.

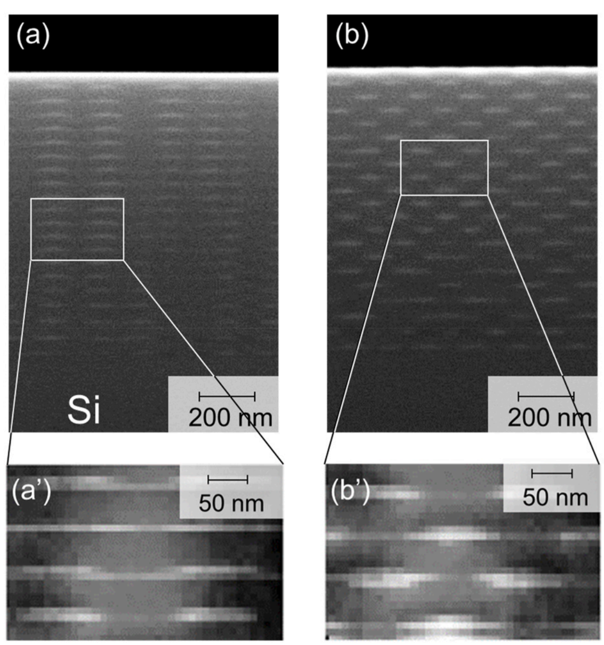

Fig. 2. (a, b) Typical cross–sectional SEM and (a', b') HAADF–STEM images of SiGe–NDs embedded in Si Structures. Si spacers were deposited using (a, a') SiH_2Cl_2 or (b, b') SiH_4.

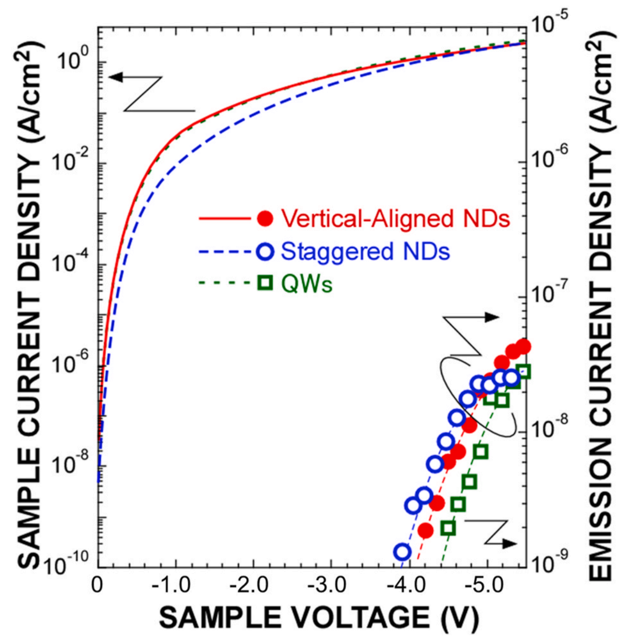

Fig. 3. Sample current and emission current–sample voltage characteristics of the vertical–aligned, and staggered SiGe–NDs. The acceleration voltage was kept constant at 40 V. A reference is provided with a 20–stacked SiGe–MQWs.

wet–cleaning steps, ~50–nm–thick Si layers were epitaxially grown on the n–Si(100) substrate using SiH_4 via RP–CVD. Subsequently, SiGe–NDs with a Ge content of 35% were deposited at 550 °C using a mixture of SiH_4 and GeH_4 gases. Growth rate of the SiGe layer is 6.6 nm/min And nominal target SiGe thickness is 5 nm. The SiGe–NDs were then covered with a 50–nm–thick Si spacer, which was deposited using SiH_2Cl_2 or SiH_4 to form dot–on–dot aligned and staggered SiGe–NDs, respectively. By repeating the deposition of SiGe–NDs and the Si spacers, 20–stacked SiGe–NDs embedded in Si structures were formed. We also fabricated a 20–stack SiGe quantum well (QW) structure as a reference. For the SiGe–multi–QW growth, same process condition as the SiGe–ND depositions was used. To prevent SiGe–ND formation, reduced process temperature by 50 °C using SiH_4 is selected for the following Si spacer depositions to prevent SiGe–ND formation by Stranski–Krastanov mechanism. After forming SiGe–ND and QW multiple–stack structures, ~5.0–nm–thick SiO_2 layers were formed using atomic layer deposition (ALD). After that, Au top–electrodes, and subsequent Al contact were formed by thermal evaporation through a stencil mask, where the size of Au–electrode and Al–contact pad was ~4.13, and ~1.15 mm^2, respectively. Finally, Al backside–contact electrode was formed through thermal evaporation.

Fig. 1 shows a measurement set up for electron emission. The electron emission characteristics were evaluated in the vacuum of ~10^{-2} Pa. A collector electrode with a size of ~7.85 mm^2 for electron emission current measurement was placed ~10 mm away from the sample surface, and DC bias (V_s) applied with respect to the top electrode. In this experiment, to prevent the measurement loss of electron emission current caused by secondary electron emission, porous gold film was used for the collector electrode, as shown in the inset Fig. 1, and acceleration bias (V_{acc}) was applied with respect to the top electrode.

3. Results and discussion

Fig. 2 shows cross–sectional scanning electron microscopy and high–angle annular dark–field (HAADF) scanning transmission electron microscopy (STEM) images of 20–stacked SiGe–NDs embedded in Si structures. The images depict the formation of vertically aligned and staggered 20–stacks of SiGe–ND structures. The estimated dot heights are ~15 and ~20 nm for the vertical–aligned and staggered NDs, respectively. For both samples, no misfit dislocation formations are observed indicating pseudomorphic growth of the SiGe–ND. Well––ordered SiGe–ND alignment is indicating regular periodic strain distribution, i. e. no irregular fluctuations around the dislocations are existing in the STEM images. The SiGe–NDs are compressively strained. Strain distributions of Si spacers on the SiGe–ND layer is tensile above the embedded SiGe–NDs, compressive above the edge of the SiGe–NDs and neutral between the embedded NDs. Detailed strain distribution is described in Ref. 36.

Fig. 3 shows the sample current (I_s) and electron emission current (I_e) densities of the vertical–aligned–ND stacks as a function of DC bias (V_s)

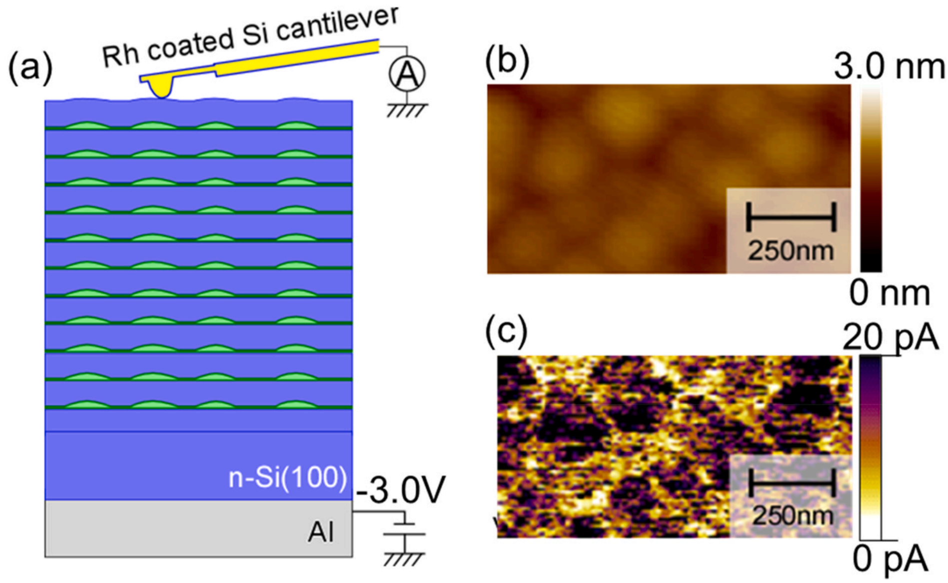

Fig. 4. (a) Experimental setup for the conductive AFM measurement, (b) AFM topographic image, and (c) corresponding current images for the vertical–aligned SiGe–NDs. The current image was taken by applying a bias of −3.0 V to the substrate.

while keeping the acceleration bias constant at 40 V. As DC bias increases in the negative bias direction, the sample current also increases. Electron emission is observed when the sample voltage exceeds ∼−4 V. In addition, the emission current was exponentially increased with an increase in the $|V_s|$ when the negative bias exceeds a threshold value of electron emission. No electron emission is observed under positive bias conditions. We also confirmed that electron emission current was hardly detected for the stacked–ND structures without ALD–deposited SiO_2, which indicates that formation of the SiO_2 layer on the dots–stacked structures effects on the electron emission from the dots. Notably, for the QWs, electron emission is detected at an applied bias over −4.5 V, with no significant change in the current level compared to the vertical–aligned NDs. However, the electron emission current of the QWs was slightly lower than that of the vertical–aligned NDs.

To clarify where electrons were emitted from the vertical–aligned NDs structure, namely, the difference in electron concentration between vertical–aligned NDs and the spaces in–between, topographic and current images were simultaneously measured using atomic force microscopy (AFM) with a conducting probe at −3.5 V applied to the backside contact relative to the tip. Fig. 4 shows a clear correlation between the topographic and current images. Unlike the topographic images, the current image reveals distinct contrast between NDs and the spaces. In this experiment, surface roughness is ruled out as a factor affecting the current since there is no significant difference between the current levels obtained in the current image and those obtained in point contact current–voltage characteristics on the ND and the Si–spacer surfaces with a conducting probe. Therefore, the results obtained from the local electron transport measurements indicate electron conduction through the protrusions in the direction of the film growth, especially the vertical–aligned NDs, which dominate electron transport owing to the difference in electron concentration between the SiGe–NDs and the Si spaces. Considering the energy level difference of the valence band between the strained SiGe–ND and the Si spacer, as well as the quantum confinement effect of the NDs reported in ref [37], electron emission from the SiGe–NDs may be attributed to their deep potential well.

We also evaluated the electron emission properties of the staggered NDs and found that electron emission is observed for the staggered NDs at an applied bias of −3.95 V and over, as shown in Fig. 3. The threshold value of the emission current is almost the same as that of the aligned NDs although the sample current decreased slightly for the staggered NDs in spite of the region of series resistance of the device. This result

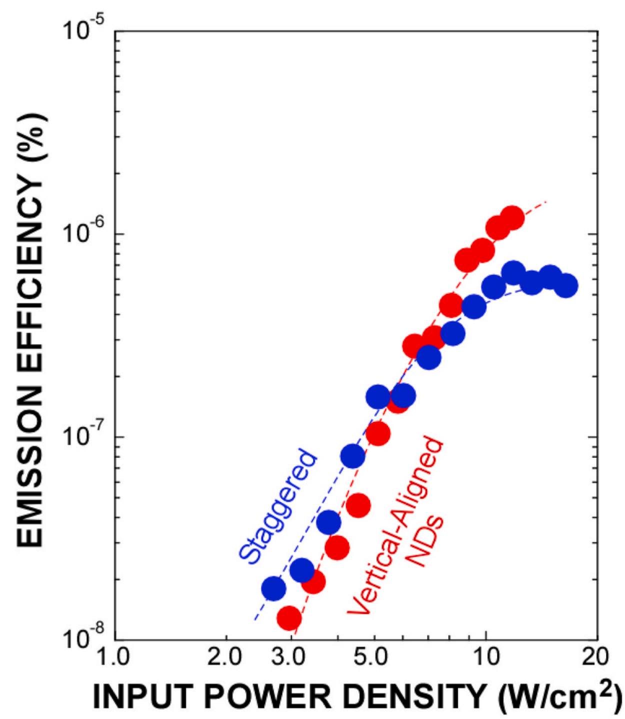

Fig. 5. Input power dependence electron emission currents for the staggered and vertical–aligned SiGe–NDs, with a constant acceleration bias of 40 V.

indicates a decrease in the electron injection rate from the n–Si(100) to the staggered NDs. Based on these results, we summarized the emission current efficiency as a function of input power, which was calculated as sample bias × sample current density described in Fig. 3, at an acceleration bias of 40 V, as indicated in Fig. 5. Stable electron emission was obtained at lower input powers for the staggered NDs compared to the aligned NDs. It should be noted that the emission current tends to saturate with increased input power. To clarify the saturation of electron emission current, we also measured its dependence on acceleration bias while keeping the sample bias at −5.0 V. The results clearly indicate an increase in the emission current with an increase in the acceleration

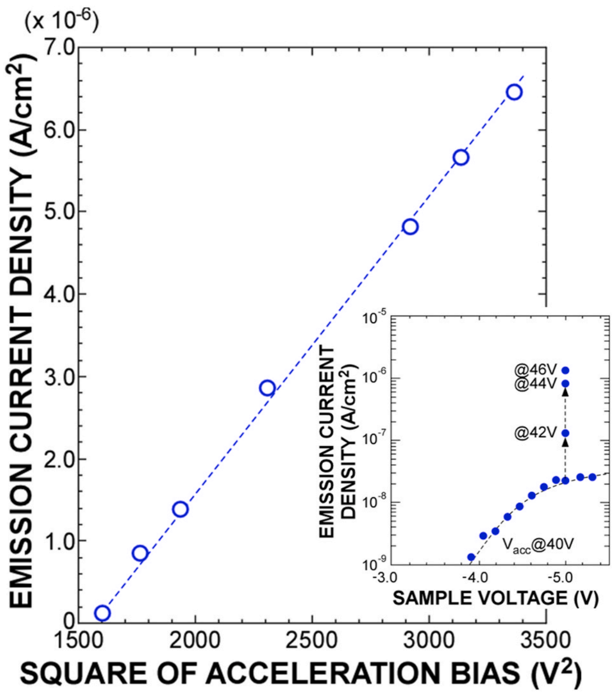

Fig. 6. Emission current density for the staggered SiGe–NDs measured at a sample bias of −5.0 V as a function of square of acceleration bias. Emission current densities measured at different acceleration biases with keeping a sample bias at −5.0 V were also shown in the inset.

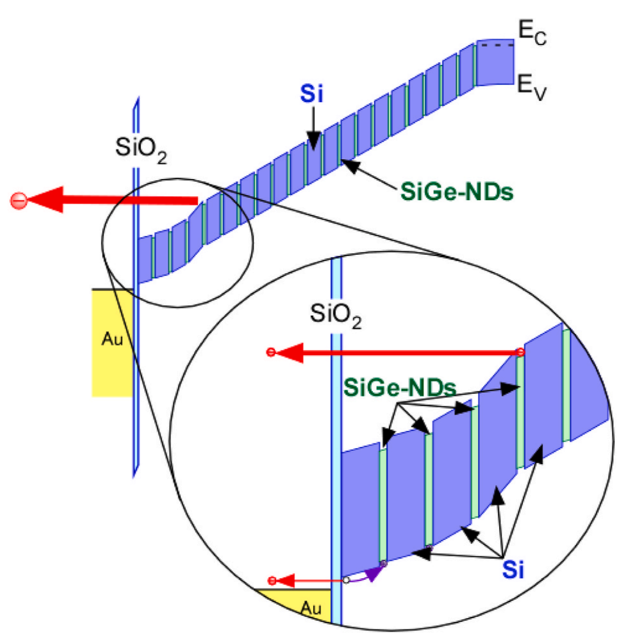

Fig. 7. Energy band diagrams at −5.0 V of the 20–fold–stacked SiGe–NDs.

bias. Thus, we summarize the emission current as a function of the square of acceleration bias, as shown in Fig. 6. The emission current is proportional to the square of the acceleration bias. Hence, the saturation of electron emission at −5.0 V and over can be attributed to the formation of a space charge because the space–charge–limited current J is given by the following equation;

$$J = \frac{8\varepsilon_i \mu}{9d^3} V^2$$

where ε_i, μ, and d are insulator dynamic permittivity, carrier mobility, and insulator thickness, respectively, and V is applied bias. The observed electron emission from the SiGe–ND stacks can be attributed to the electric field concentration on the upper layers of SiGe–NDs, resulting from the accumulation of holes in the deep potential well of the SiGe–ND. This accumulation facilitates the extraction of valence electrons and enhances electron injection from the substrate, as schematically illustrated in Fig. 7. In addition, the improved electron emission efficiency of the staggered NDs under the low input power operation below ~5.0 W/cm^2 can be explained by the reduced current leakage associated with the staggered structure. These results indicate that vertical–aligned SiGe–ND structures effectively enhance electron emission under high–voltage conditions, while staggered NDs are suitable for low–voltage operation at a low acceleration bias condition.

4. Conclusion

We have demonstrated that stable electron emission from the multiple stacked SiGe–NDs embedded in Si/n–Si(100) structures when the negative bias was applied to the bottom electrode with respect to the grounded top electrode over a threshold bias. Notably, the electron emission efficiency was markedly enhanced for staggered SiGe–NDs compared to the vertical–aligned SiGe–NDs under the low–voltage operation at a low acceleration bias condition. This enhancement can be attributed to a decrease in current leakage.

CRediT authorship contribution statement

Katsunori Makihara: Writing – original draft, Project administration, Investigation, Funding acquisition, Formal analysis, Conceptualization. **Yuji Yamamoto:** Writing – review & editing, Investigation, Formal analysis. **Hiroya Yagi:** Formal analysis. **Lingrui Li:** Formal analysis. **Noriyuki Taoka:** Data curation. **Bernd Tillack:** Supervision. **Seiichi Miyazaki:** Supervision.

Declaration of competing interest

The authors have no conflicts of interest directly relevant to the content of this article.

Data availability

No data was used for the research described in the article.

Acknowledgements

This work was supported in part by Grant–in–Aid for Scientific Research (A) 19H00762, 21H04559, and Fund for the Promotion of Joint Intentional Research [Fostering Joint International Research (A)] 18KK0409 of MEXT Japan. Another would like to thank IHP−Leibniz−Institut für innovative Mikroelektronik cleanroom staff epitaxy process team for the fabrication of samples and their excellent support.

References

[1] R. Apetz, L. Vescan, A. Hartmann, C. Dieker, H. Lüth, Appl. Phys. Lett. 66 (1995) 445–447.
[2] O.G. Schmidt, K. Eberl, IEEE Trans. Electron Devices 48 (2001) 1175–1179.
[3] A.A. Dadykin, YuN. Kozyrev, A.G. Naumovets, J. Exp. Theor. Phys. Lett. 76 (2002) 472–474.
[4] A. Alguno, N. Usami, T. Ujihara, K. Fujiwara, G. Sazaki, K. Nakajima, Y. Shiraki, Appl. Phys. Lett. 83 (2003) 1258–1260.
[5] B.-C. Hsu, S.T. Chang, T.-C. Chen, P.-S. Kuo, P.S. Chen, Z. Pei, C.W. Liu, IEEE Electron. Device Lett. 24 (2003) 318–320.
[6] P.S. Chen, Z. Pei, Y.H. Peng, S.W. Lee, M.-J. Tsai, Mater. Sci. Eng., B 108 (2004) 213–218.
[7] K.L. Wang, D. Cha, J. Liu, C. Chen, Proc. IEEE 95 (2007) 1866–1883.

[8] S. Cosentino, P. Liu, S.T. Le, S. Lee, D. Paine, A. Zaslavsky, D. Pacifici, S. Mirabella, M. Miritello, I. Crupi, A. Terrasi, Appl. Phys. Lett. 98 (2011) 221107.
[9] X. Xu, N. Usami, T. Maruizumi, Y. Shiraki, J. Cryst. Growth 378 (2013) 636–639.
[10] A. Samavati, Z. Othaman, S.K. Ghoshal, M.R. Dousti, J. Lumin. 154 (2014) 51–57.
[11] X. Xu, T. Maruizumi, Y. Shiraki, Opt Express 22 (2014) 3902–3910.
[12] M. Grydlik, F. Hackl, H. Groiss, M. Glaser, A. Halilovic, T. Fromherz, W. Jantsch, F. Schäffler, M. Brehm, ACS Photonics 3 (2016) 298–303.
[13] A.I. Yakimov, V.V. Kirienko, A.A. Bloshkin, V.A. Armbrister, A.V. Dvurechenskii, J.-M. Hartmann, Opt Express 25 (2017) 25602–25611.
[14] M. Brehm, M. Grydlik, Nanotechnology 28 (2017) 392001.
[15] K. Makihara, M. Ikeda, N. Fujimura, K. Yamada, A. Ohta, S. Miyazaki, APEX 11 (2017) 11305.
[16] J.W. John, V. Dhyani, S. Singh, A. Jakhar, A. Sarkar, S. Das, S.K. Ray, Nanotechnology 32 (2021) 315205.
[17] S. Shi, D. Pacifici, A. Zaslavsky, Appl. Phys. Lett. 119 (2021) 221108.
[18] Q. Chen, L. Zhang, Y. Song, X. Chen, S. Koelling, Z. Zhang, Y. Li, P.M. Koenraad, J. Shao, C.S. Tan, S. Wang, Q. Gong, ACS Appl. Nano Mater. 4 (2021) 897–906.
[19] P. Krause, J.C. Tremblay, A. Bande, J. Physical chemistry A 125 (2021) 4793–4804.
[20] M.S. Storozhevykh, L.V. Arapkina, S.M. Novikov, V.S. Volkov, A.V. Arsenin, O. V. Uvarov, V.A. Yuryev, J. Raman Spectrosc. 53 (2022) 853–862.
[21] A.A. Dadykin, YuN. Kozyrev, A.G. Naumovets, J. Exp. Theor. Phys. Lett. 76 (2002) 472–474.
[22] S.D. Hutagalung, K.A. Yaacob, Y.C. Keat, Solid State Phenom. 121–123 (2007) 529–532.
[23] J. Xu, J. Zhou, Y. Yao, Z. Cen, F. Song, L. Xu, J. Wan, K. Chen, Solid State Commun. 145 (2008) 443–446.
[24] N. Koshida, T. Ohta, B. Gelloz, A. Kojima, Curr. Opin. Solid State Mater. Sci. 15 (2011) 183–187.
[25] M. Esashi A Kojima, N. Ikegami, H. Miyaguchi, N. Koshida, Microsystems & Nanoengineering 1 (2015) 15029.
[26] H. Nishino, S. Yoshida, A. Kojima, N. Ikegami, S. Tanaka, N. Koshida, M. Esashi, Electronics & Communications Jpn. 99 (2016) 11.
[27] R. Suda M. Yagi, A. Kojima, N. Mori, J. Shirakashi, N. Koshida, Mater. Sci. Semicond. Process. 70 (2017) 44.
[28] N. Koshida, T. Nakamura, Front. Chem. 7 (2019) 279.
[29] R. Suda, A. Kojima, N. Koshida, ECS J. of Solid State Sci. and Tech. 7 (2018) Q222–Q227.
[30] V. Le Thanh, V. Yam, Y. Zheng, D. Bouchier, Thin Solid Films 380 (2000) 2–9.
[31] D. Grützmacher, T. Fromherz, C. Dais, J. Stangl, E. Müller, Y. Ekinci, H.H. Solak, H. Sigg, R.T. Lechner, E. Wintersberger, S. Birner, V. Holý, G. Bauer, Nano Lett. 7 (2007) 3150–3156.
[32] W.C. Wen, M.A. Schubert, M.H. Zöllner, B. Tillack, Y. Yamamoto, ECS Trans. 109 (2022) 343.
[33] W.C. Wen, M.A. Schubert, M.H. Zoellner, B. Tillack, Y. Yamamoto, ECS J. Solid State Science and Technology 12 (2023) 055001.
[34] Y. Yamamoto, Y. Itoh, P. Zaumseil, M.A. Schubert, G. Capellini, K. Washio, B. Tillack, ECS J. Solid State Sci. Technol. 8 (2019) P190–P195.
[35] Y. Yamamoto, P. Zaumseil, G. Capellini, M. Andreas Schubert, A. Hesse, M. Albani, R. Bergamaschini, F. Montalenti, T. Schroeder, B. Tillack, Nanotechnology 28 (2017) 485303.
[36] Y. Yamamoto, Y. Itoh, P. Zaumseil, M.A. Schubert, G. Capellini, F. Montalenti, K. Washio, B. Tillack, Semicond. Sci. Technol. 33 (2018) 114014.
[37] M.V. Fischetti, F. Gámiz, W. Hänsch, J. Appl. Phys. 92 (2002) 7320–7324.